Materials and Design 160 (2018) 591–600

Contents lists available at ScienceDirect

Materials and Design

journal homepage: www.elsevier.com/locate/matdes

Synthesis and characterisation of floatable magnesium alloy syntactic foams with hybridised cell morphology

Akeem Damilola Akinwekomi [a,c], Chak-Yin Tang [a,*], Gary Chi-Pong Tsui [a], Wing-Cheung Law [a], Ling Chen [a], Xu-Sheng Yang [a], Mohd Hamdi [b]

[a] Department of Industrial and Systems Engineering, The Hong Kong Polytechnic University, Hung Hom, Kowloon, Hong Kong, China
[b] Centre of Advanced Manufacturing and Material Processing, Department of Mechanical Engineering, Faculty of Engineering, University of Malaya, Kuala Lumpur 50603, Malaysia
[c] Department of Metallurgical and Materials Engineering, Federal University of Technology, PMB 704 Akure, Ondo State, Nigeria

HIGHLIGHTS

- Magnesium alloy AZ61 syntactic foams with hybrid pore structure were fabricated via microwave sintering techniques.
- Floatable magnesium alloy AZ61 syntactic foam was realised with a density 0.79 g/cm^3 and adequate strength.
- The whole process of microwave sintering is within 20 minutes, minimizing the interfacial reactions and energy consumption.
- Potential applications as a floatable metallic microboat and chemical release agent were demonstrated.

GRAPHICAL ABSTRACT

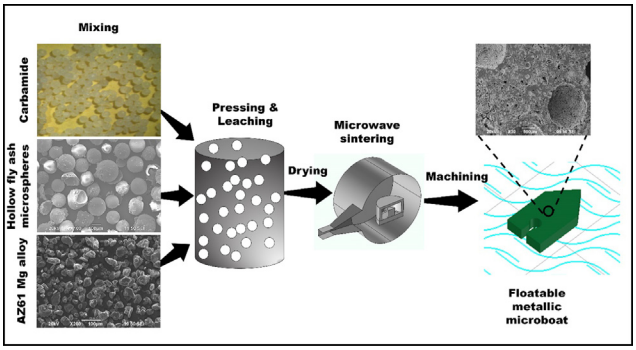

ARTICLE INFO

Article history:
Received 15 June 2018
Received in revised form 2 October 2018
Accepted 4 October 2018
Available online 4 October 2018

Keywords:
Magnesium alloy
Powder metallurgy
Microwave sintering
Mechanical properties
Syntactic foam
Hybrid cells

ABSTRACT

Powder metallurgy and rapid microwave (MW) sintering techniques were successfully applied to engineer a hybrid cell structure into magnesium alloy AZ61 syntactic foams. The hybrid cell structure, comprising open- and closed-cells, originated from leached carbamide granules and hollow microspheres of fly ash (HS), respectively. External MW susceptors accelerated the sintering process and greatly mitigated the formation of undesirable interfacial reactions. The cell hybridisation technique facilitated control over the density and strength of the syntactic foams. Accordingly, floatable syntactic foams with a density of about 0.79 g/cm^3 and compressive strength of 16 MPa were synthesised without recourse to any surface modification or chemically-induced superhydrophobicity. The processing techniques were capable of mitigating damage to the HS microspheres as confirmed by microstructural examinations. Furthermore, potential applications of the floatable syntactic foam sample, as a microboat and chemical release agent, were demonstrated by using ethanol as a propellant. AZ61 syntactic foams synthesised in this study exhibited low density and adequate strength, suggesting their applicability as alternative materials to polymer composite foams.

1. Introduction

Magnesium (Mg)-based syntactic foams are two-phase composite materials having hollow spheres (HS) embedded in an Mg matrix. On account of their lightweight, they can be useful for minimising

* Corresponding author.
E-mail address: cy.tang@polyu.edu.hk (C.-Y. Tang).

https://doi.org/10.1016/j.matdes.2018.10.004

structural weight [1,2]. Other applications include electromagnetic shielding in electronics [3], damping and energy absorption [4]. Generally, metal matrix syntactic foams (MMSFs) exhibit higher moduli and strength as compared to individual open and closed-cell foams with similar porosity levels, due to the reinforcement provided by the shells of the hollow spheres [5–9]. Fly ash (HS) is a commonly used hollow microspheres because it is cheap and readily available as an industrial waste from coal thermal stations.

The walls of fly ash HS particles are thin, weak, and contain micropores, thus they are easily damaged during composite processing [6,10]. Mg-based syntactic foams can be fabricated through stir casting or pressure infiltration during melt processing. However, these techniques can damage the fragile HS particles and lead to melt-infiltration into the hollow cavities of the particles due to the force from mechanical stirring and the applied infiltration pressure [2,11,12]. This defeats the goal of achieving low density. Moreover, high reactivity of Mg matrix leads to excessive formation of interfacial products that subsequently deplete the shell material of hollow spheres and reduce their strengthening effect [6].

The solid-state powder metallurgy (PM) processing route is a viable alternative that can overcome some of these challenges, due to its versatility in accommodating a high volume fraction of reinforcement particles, near-net shape capability and lower processing temperature [7,13]. Nevertheless, this route is seldom utilised for fabricating MMSFs because a high compacting pressure can easily fracture the HS particles during composite processing. Conversely, a low pressure will form samples with low green strength that are difficult to handle during the subsequent processing stages. Prolonged sintering cycles of several hours add to the production cost and lead to the formation of undesirable brittle interfacial products. Thus, there have been only a few reports utilising this technique [6,7,14]. As a result, microwave (MW) sintering is emerging as an alternative and rapid sintering technique, which can significantly reduce processing time and energy consumption [15–17]. MW sintering, due to its rapid heating rate, can help to minimise deleterious reactions between Mg and HS. Therefore, the hollow particles can contribute to strengthening while their hollow structure can be utilised for functional applications, such as buoyant micro-robots and chemical release agents.

MMSFs can withstand large compressive deformations, so they are traditionally utilised in energy absorption applications [8]. Cell hybridisation offers an opportunity to customise the properties of MMSFs for other applications, such as floatability and electromagnetic interference shielding. In recent years, a few studies on different metal matrices have been reported based on this approach [18,19]. Hybrid cells, formed from a gas releasing agent and HS hollow spheres, were incorporated into a zinc alloy Zn12Al matrix [18]. Foams with a hybrid cell structure possessed higher yield and plateau strengths compared with gas-foamed Zn12Al foams. Similarly, aluminium alloy LM13/HS syntactic foams with fly ash HS were fabricated via a stir casting method [19]. The processing temperature influenced the cell morphology which resulted in the formation of hybrid foams with a mixture of partially opened and closed-cells. Prior to this current investigation on MMSFs, there has been no such previous study on Mg-based syntactic foams having a hybrid cell structure and with floatability or buoyancy functionality.

Floatable mini- or micro-devices, such as microboats, have potential applications as mixers, sensors, rotors, cargo/drug delivery, and micro robots [20]. Hence, the main choice of materials are polymers, whose densities are lower than that of water or are light enough to be supported by the surface tension of water [21–23]. Earlier studies on buoyant metallic structures, such as porous copper foam [24] and robotic water strider with copper wire legs [25], utilised modification of surface chemistry and increasing surface roughness to induce superhydrophobicity and/or superoleophobicity. However, these surfaces degrade with time, suffer from instability, and are mechanically weak [26]. Furthermore, the modification processes are, most times, tedious and protracted. Mg, due to its low density, is expected to exhibit very low density and higher specific properties when processed as a foam. Herein, a proposed cell hybridisation technique was used to engineer a hybrid cell structure into an AZ61 Mg alloy to form AZ61/fly ash syntactic foam. This technique was utilised to reduce the density of the syntactic foam sample and achieve its floatability on water while still exhibiting adequate strength. With this technique, neither chemical nor surface modification techniques were required to achieve floatability. The effects of the volume fractions of fly ash HS microspheres and leachable carbamide granules on the density, compression and energy absorption properties of the synthesised syntactic foams were studied. The syntactic foams synthesised in this study are lightweight and can serve as alternative materials to polymer composite foams. Potential applications, as a microboat and chemical release agent, were also demonstrated.

2. Materials and methods

2.1. Materials

Magnesium alloy AZ61 powder (150–300 μm, Tangshan Weihao Magnesium Powder Co., Ltd., China) served as the matrix material while commercially available spherical carbamide granules (CB; $(CO(NH_2)_2)$; 0.50–0.90 mm) were used as space holder agents to create the open cell structure. To enhance MW sintering, the average particle size of the AZ61 powder was reduced to about 50 μm by mechanically milling. Details of the milling process have been published elsewhere [15].

Fly ash hollow microspheres (HS) were used as space holders for generating closed cells in the matrix. HS microspheres had a density of 0.70 g/cm^3 and were basically spherical in shape (Ø 100–250 μm) with a wall thickness of 16.08 ± 7.70 μm. Prior to using the HS, they were pre-treated in 1 M potassium hydroxide (KOH) solution for 1 h at 120 °C to dissolve any organic matter that might be present. Moreover, KOH solution can retard the crystallisation of zeolite due to the presence of K^+ ions [27]; therefore, the structural integrity and shape of the shell could be preserved. Fig. 1 shows the microstructure of HS microspheres. The main chemical constituents of HS (aluminosilicates), with other trace minerals, are also shown in Table 1.

2.2. Synthesis of Mg alloy AZ61 syntactic foams with a hybrid cell structure

Two groups of samples were designed and fabricated for achieving a theoretical density less than that of water (i.e. 1.00 g/cm^3). The influence of the HS and CB volume fractions on the density, microstructure and strength of the syntactic foams were investigated. In *Group 1*, the volume fractions of HS were varied while the ratio of the volume fractions of AZ61 to CB were kept constant at 3:2; thus, syntactic foams with 20, 30, and 40% HS were fabricated. Conversely, *Group 2* samples had the volume fractions of AZ61 and HS maintained at a constant ratio of 3:2, while the volume fractions of CB were varied as 20, 30, and 40% CB.

Samples of the AZ61/CB/HS mixture were mixed for 20 min with ~2 mL of ethanol to moisten the surfaces of HS and CB and minimise particle segregation. In order to preserve the sphericity and hollowness of the HS microspheres, the compaction pressure for forming green samples was estimated based on the load/pressure partitioning relationship and assuming that only AZ61 and HS were present, because CB will be eventually leached out from the mixture:

$$P_c = \sigma_m V_{f,m} + \sigma_{HS} V_{f,HS} \quad (1)$$

where, P_c is the compaction pressure, σ_m is the yield strength of the matrix (130 MPa), σ_{HS} is the yield strength of fully compacted HS (600 MPa [14]), and V_f is the volume fraction. However, the HS shell contained

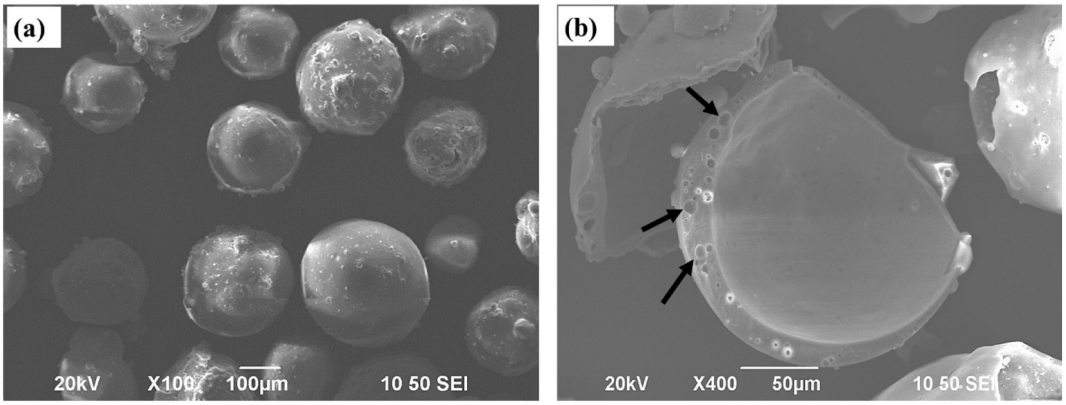

Fig. 1. SEM microstructural images of (a) fly ash hollow sphere particles and (b) micropores (black arrows) in the shell of a fractured fly ash particle.

some micropores (Fig. 1b), which further reduced its strength. To account for this, Eq. (1) was modified as follows [14]:

$$P_c = \sigma_m V_{f,m} + \sigma_{HS} V_{f,HS}\left[C \times \left(1 - V_{void,HS}\right)^n\right] \quad (2)$$

where C and n are the material constants and $V_{void,\,HS}$ is the void fraction in HS, and it can be further expressed as:

$$V_{void,HS} = \frac{\rho_{c,HS} - \rho_{HS}}{\rho_{c,HS}} \quad (3)$$

where $\rho_{c,\,HS}$ is the density of fully compacted HS (~1.90 g/cm^3) and $C = 0.75$ and $n = 2.19$ [14]. The ratio of the volume fractions of AZ to HS is 1.50. Therefore, P_c was approximated to about 100 MPa. Additional 20 MPa was added to account for the frictional resistance from the die wall and powder mixture during pressing. The AZ61/CB/HS mixture was put in a rigid cylindrical die and uniaxially pressed at 120 MPa for 2 min to form green samples. This low compaction pressure is expected to preserve the hollowness of the fly ash HS microspheres and form green samples with adequate green strength for handling in the subsequent processing steps. Open cells were created in the samples by leaching CB in deionised (DI) water maintained at room temperature for 3 h. Subsequently, the porous samples were dried at 150 °C for 3 h prior to MW sintering.

2.3. Microwave sintering and X-ray diffraction (XRD) analyses

Green samples were sintered in a 2.45 GHz HAMiLab-HV3 high vacuum multimode MW furnace (SYNOTHERM Corporation). Temperature was monitored using a non-contact infrared Raytek pyrometer (Marathon 2MH model). Due to the small size of the sample (Ø 15 mm), moderate thermal conductivity of Mg, and volumetric heating characteristic of MW sintering, temperature gradient across the sample is expected to be minimal. A steady sintering temperature was maintained by automatically adjusting the MW power between 100 and 350 W. The samples were sintered using a susceptor-mediated hybrid MW sintering technique. The sintering was carried out at 500 °C in an atmosphere of flowing high purity argon gas for 20 min. Due to the poor MW absorption of Mg at ambient temperature, external heating from a susceptor, comprising a hybrid mixture of silicon carbide and graphite, was utilised to increase the temperature of the green compacts until they began to couple and absorb MWs. Therefore, the samples underwent volumetric heating and sintering proceeded at a rapid rate. X-ray diffraction studies (Rigaku SmartLab 9 kW XRD equipment) were performed on the sintered syntactic foam samples to identify the phases in the microstructure. The samples were exposed to Cu Kα radiation (λ = 1.54056 Å) at a scanning speed of 4°/min.

Table 1
Chemical composition of hollow sphere (HS) particles.

Chemical composition	Al_2O_3	SiO_2	Fe_2O_3	CaO	MgO	K_2O	Na_2O
Weight fraction (%)	33–38	56–62	2–4	0.2–0.4	0.8–1.2	0.5–1.1	0.3–0.9

2.4. Density and microstructural characterisations

The sintered density of each composite group was determined by mass and dimensional measurements. A minimum of five samples were measured and the average result was reported as the density. Microstructural observation was carried out using a scanning electron microscope (SEM, JEOL JSM-6490).

2.5. Compression and energy absorption characterisations

Uniaxial compression tests were performed on cylindrical samples having a height-to-diameter ratio of 1.5 using an MTS810 universal testing machine with a crosshead speed of 1 mm/min at ambient temperature. A minimum of five specimens were tested for each set to get an average result and to assess the repeatability of the experimental procedure and the results. The stress–strain curve was used to determine the compressive strengths of the foams, while their energy absorption capacities were estimated from the area under the stress-strain curve up to 40% strain.

2.6. Potential application of floatable AZ61 syntactic foam as a microboat

2.6.1. Surface wetting characterisation and fabrication of a microboat

Static water contact angle (CA) of the surface of an AZ61 sample was measured using a 5 μL Sessile water droplet on a Sindatek 100SL Goniometer at ambient conditions. The average of five readings was reported as the CA. A wire electrical discharge machine (Acro Star II WEDM, Acro Machinery & Electric Co., Ltd., Taiwan) was used to cut the shape of a microboat from a sintered sample (*Group 2*, 40% CB sample).

2.6.2. Propulsion and volumetric flow rate tests

Aqueous solutions of ethanol (100, 90, and 80% v/v) were used as propellants for driving the microboat. About 15 μL of ethanol solution was injected into a tiny polymeric foam (3.80 mg) and placed inside the slot at the aft of the microboat. The propulsion test was conducted in a 30 mm-deep distilled water in a rectangular plastic tank (260 × 180 × 60 mm^3). In some tests, the propellant was dyed with a blue ink to visualize the track of the microboat and to measure the volumetric flow rate of ethanol. The volumetric flow rate of ethanol was derived by immobilising the microboat and video-taping the flow of the leading edge of coloured ethanol. The video was then analysed to extract

information about the maximum velocity (v_{max}) of the leading edge of the blue ink. The experiment was repeated a minimum of three times for each concentration. The motion of the microboat was captured with a Canon PowerShot A810 digital camera at a frame rate of 25 fps. The videos were analysed using a publicly available image analysis software (ImageJ v. 1.71q) and an MTrackJ plugin [28] was used to extract the displacement and velocity of the microboat.

3. Results and discussions

3.1. Microwave sintering and X-ray diffraction analyses

AZ61 syntactic foams, with a hybrid cell structure, were successfully synthesised using the PM technique and consolidated by a rapid MW sintering scheme. As MW sintering was completed within 20 min, a remarkably shortened sintering time was achieved as compared with similar earlier studies on synthesising Mg-based foams which took 2 h [29] and 6 h [13].

A vast majority of the earlier studies on Mg-based syntactic foams were processed based on the melt processing technique [2,11,12]. In the study conducted by Newsome et al. [12], Mg alloy AZ91D/Al_2O_3 HS syntactic foams were fabricated by pressure infiltration with a melting time of about 1 h at 650 °C. Other similar studies reported processing temperature of 750 to 790 °C [2,11]. In our study, the sintering temperature was 500 °C, with a reduction of about 30% and 58%, as compared with some earlier works on AZ91/Al2O3 syntactic foams [12] and AZ91D/HS foams [11], respectively. This reduction in processing temperature can lower energy consumption, processing time, and minimise the interfacial reactions between the matrix and the HS microspheres. Although one study reported MW-sintering of Mg/HS composites [7], the sintering temperature was 640 °C and was 28% higher than utilised in our present study.

The XRD patterns of sintered hybrid cell foam samples with 20, 30, and 40% HS porosities are respectively shown in Fig. 2. Apart from the prominent peaks of the Mg matrix, which were present in all the samples, peaks belonging to MgO, $Al_{12}Mg_{17}$ and Mg_2Si were also identified. These phases were also observed in sintered Mg-fly ash composites [7] and melt processed AZ91-fly ash syntactic foams [11]. The formation of Mg_2Si and MgO is due to the reactions between the Mg (matrix) and HS (mainly made up of Al_2O_3 and SiO_2). The possible reactions [30–32] are given below:

$$3\,Mg + Al_2O_3 \rightarrow 3MgO + 2Al \quad (4)$$

$$2\,Mg + SiO_2 \rightarrow 2MgO + Si \quad (5)$$

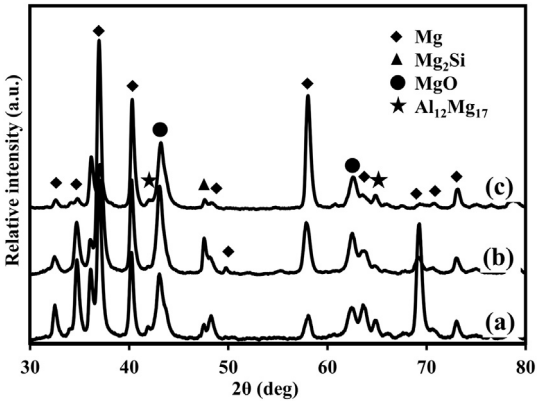

Fig. 2. XRD patterns of hybrid cell foams with HS volume fraction of (a) 20%, (b) 30%, and (c) 40%, respectively.

Due to the excess Mg present in the matrix [32], the reaction in Eq. (6) proceeds further as:

$$2\,Mg + Si \rightarrow Mg_2Si \quad (6)$$

As observed from the XRD result in Fig. 2, no peaks belonging to carbamide could be seen. It could, therefore, be concluded that the leaching process eliminated all the carbamide granules. The choice of carbamide as an open cell former over sodium chloride (NaCl) was informed by its benign corrosion effect on Mg during the dissolution stage. NaCl space holders, however, have been reported to exacerbate the corrosion of Mg-based foams [33]. Although carbamide leaching in DI water was carried out for 3 h, no significant corrosion products, such as Mg(OH)2, could be identified from the diffraction patterns. This indicated that the leaching process imparted minimal corrosion to the Mg matrix. The long leaching process was required due to the presence of HS particles in the matrix that could possibly shield CB granules from dissolving in DI water. Any undissolved CB could react with Mg during the sintering stage, as reported by Zhuang et al. [34] and affect mechanical strength.

3.2. Density and microstructural characterisations

The results of the sintered density and porosity of the syntactic foam samples are presented in Table 2.

The sintered densities of the syntactic foams were generally very close to 1.00 g/cm^3, with a group of the samples (40% CB) showing a significantly lower value. Unlike the density of the samples in *Group 2*, it was observed that the sintered densities of the samples in *Group 1* increased with an increase in the volume fraction of HS in the matrix. Additionally, the sintered densities (*Group 1*) were noted to be slightly higher than the estimated theoretical densities. This discrepancy between the theoretical and experimental densities has also been reported in some previous studies [7,35].

In the earlier publication [35], the reason for the discrepancy was attributed to the melt-filled and broken HS microspheres, whereas, in the later study [7], the authors attributed the discrepancy to the presence of broken HS microspheres in the matrix during extrusion. However, neither extrusion nor melt processing was undertaken in our report. Therefore, it was postulated that the formation of Mg_2Si and MgO, due to the reaction between Mg and HS, was responsible for the increase in the sintered densities of *Group 1* samples.

The analysis of the X-ray diffraction patterns of the sintered specimens, shown in Fig. 2, indicated that some peaks corresponding to MgO and Mg_2Si, were present in the samples. MgO has a density of 3.58 g/cm^3 [36], while Mg_2Si has a density of 1.99 g/cm^3 [37]. Although it is challenging to quantify the proportion of these two phases in comparison to the Mg phase, the densities of these two secondary phases

Table 2
Density, compressive strength and energy absorption properties of AZ61 composite foams with hybrid pore structure.

Group	Designation	Theoretical density (g/cm^3)	Sintered density (g/cm^3)	Compressive strength (MPa)	Energy absorption (J/cm^3)
1	20% HS	1.00	0.90	25.24 ± 2.98	6.20 ± 1.69
	30% HS	0.97	0.98	30.13 ± 0.34	8.35 ± 0.55
	40% HS	0.93	1.10	16.11 ± 0.35	4.04 ± 1.20
2	20% CB	1.01	1.02	28.77 ± 4.13	7.78 ± 0.61
	30% CB	0.85	0.90	22.59 ± 3.27	6.64 ± 1.16
	40% CB	0.82	0.79	16.44 ± 1.82	4.02 ± 0.43

are both higher than the 1.80 g/cm^3 of the Mg matrix. Therefore, it can be rationalised that the sintered density of the syntactic foam increased as the volume fraction of HS increased, because more SiO_2 and Al_2O_3 (the main constituents of HS) were available for reaction with the matrix.

Furthermore, the syntactic foam samples with 40% CB showed remarkable floatability on water, to be discussed in Section 3.4, owing to their hybrid cell structure and low density of 0.79 g/cm^3. Other samples, with sintered densities lower than 1.00 g/cm^3, floated for a short while, but later sank. This was attributed to the interconnectivity of the surface cells that allowed the ingress of water into the interior cells of the samples. Sealing the surface open cells of these samples may be helpful in solving this problem. By a careful design of the open and closed-porosities through hybridisation, floatable syntactic composite foams have been fabricated. A recent study by Anantharaman et al. [1] reported the density of Mg alloy AZ91D/SiC HS syntactic foams to be about 0.97 g/cm^3. The foams were processed using a sub-atmospheric pressure infiltration route. Nonetheless, the results in Table 2 clearly show that the Mg alloy AZ61/HS syntactic foams processed in this study exhibit lower densities than previously reported for Mg-based syntactic foams [1]. Without recourse to the melt processing technique and surface modification methods, it has been demonstrated that floatable Mg syntactic foams could be processed by cell hybridisation technique through the PM and MW sintering techniques. Its potential application as a microboat is described in Section 3.5.

Fig. 3 shows the microstructural SEM images of a typical syntactic foam sample with a hybrid cell morphology. The features enclosed by white, dotted circles are the spherical cells left behind after leaching-out the CB granules prior to the sintering stage. On the other hand, intact HS microspheres are shown within the boundary of the black, dotted circles. Fig. 3(a) also confirmed that some of the HS were embedded in the walls of the large cells, which are expected to provide reinforcement and help to improve strength during loading. Some microscopic inter-particle pores (white arrows) are also seen in Fig. 3 due to the low compacting pressure utilised for pressing the samples. Similar microscopic voids present in the microstructures of sintered Al/HS syntactic foams have been reported [6].

The images in Fig. 3(b) and (c) also indicated that the HS microspheres were neither destroyed during the fabrication stage nor after the sintering stage. This can be rationalised by considering two main reasons; an optimised compaction pressure, earlier estimated by Eqs. ((1)–(3)) and compaction load-sharing by HS microspheres and CB granules during the pressing of the green samples. It should be noted that, prior to leaching CB granules, a mixture of AZ61, CB, and HS were pressed to form green samples. As such, CB granules may provide some load-bearing effect during the compaction of the green samples. Therefore, CB granules may reduce the impact of the compaction pressure on the HS microspheres and contribute to preserving their sphericity, thereby mitigating damage to their hollow structure.

The microstructural images in Fig. 3(b) and (c) of the interface between the matrix and HS showed no visible interfacial reaction products, hence, the HS were not consumed by the chemical reaction and no matrix-infiltration into HS was observed. These observations are in contrast with the remarks of some authors [3,11] utilising the melt processing technique. Significant and discernible outgrowths of Mg_2Si were observed at the interface between HS and the AZ91 matrix [11]. This massive interfacial product depleted the shell material of HS and resulted in matrix-infiltration into HS, as reported in those studies [3,11]. Prolonged conventional sintering and long residence time between HS particles and molten Mg during melt processing increase the propensity for the formation of these. In this work, as observed from the microstructural images in Fig. 3, interfacial products were

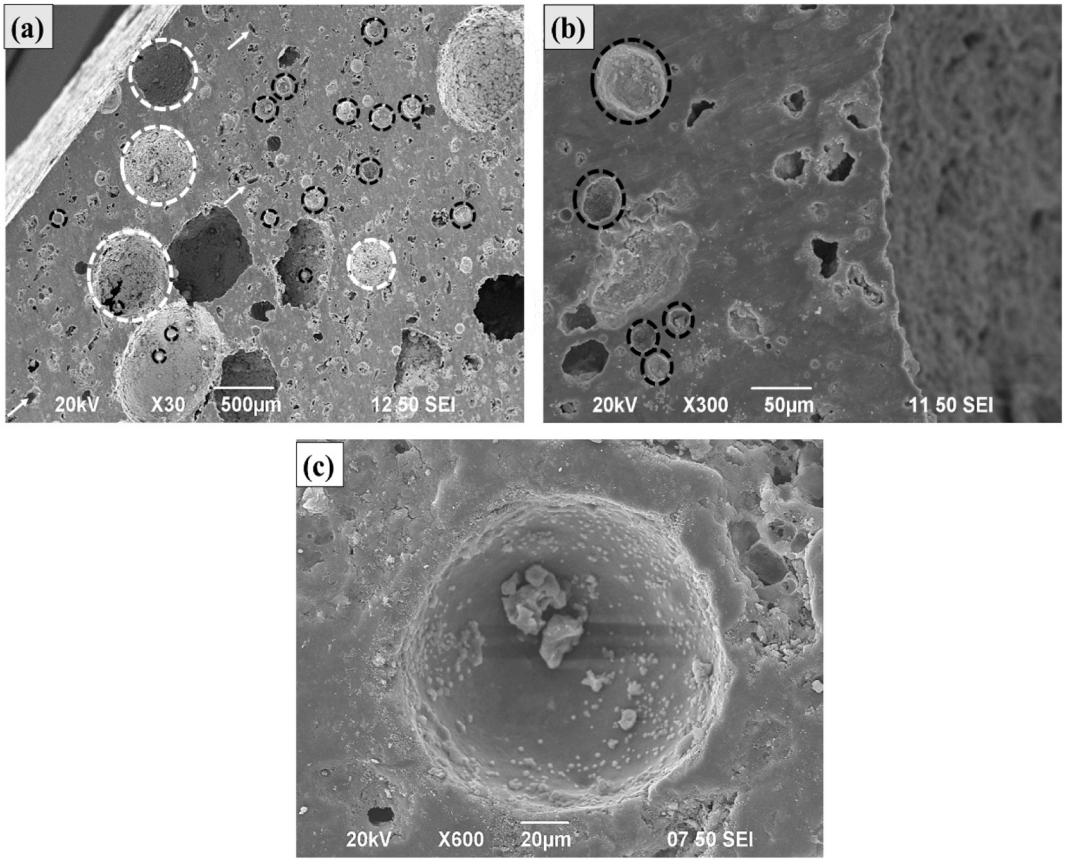

Fig. 3. Representative microstructural images of a composite foam sample with (a) hybrid cell structure (b) magnified image of (a) showing intact fly ash hollow spheres (c) interface between a fly ash particle and the matrix.

not found, indicating that rapid MW sintering minimised the formation of such interfacial products. Therefore, the result from this present study further highlights the suitability and advantages of MW sintering for processing Mg-based syntactic foams.

3.3. Compression and energy absorption characterisations

The results of the quasi-static compression tests of the foam specimens are shown in Table 2, and typical compressive stress-strain graphs in Fig. 4.

In Fig. 4, syntactic foams from both groups exhibited an initial elastic region until a certain peak strength (indicated in Table 2) was attained and then the stress dropped to an almost constant value with an increase in strain. For *Group 1* samples, with a varying HS volume fraction, the compressive strength and energy absorption capacity increased as HS was increased, with a peak at 30% HS before dropping at 40% HS. The syntactic foam sample with 30% HS exhibited the highest compressive strength of ~30 MPa and an energy absorption capacity of 8 J/cm^3. Although the highest density of 1.10 g/cm^3 was observed in the syntactic sample with 40% HS, its compressive strength was the lowest. As the volume fraction of HS was the highest in this sample, the propensity for the interfacial reaction between HS and Mg to occur may increase.

In *Group 2* samples, the 20% CB syntactic foam exhibited the highest compressive strength of about 29 MPa, while the lowest compressive strength was 16 MPa at 40% CB. Typically, the compressive strength and energy absorption capacity of *Group 2* samples were reduced as the volume fraction of CB increased. This was an expected trend, because more cells were introduced into the matrix when the volume fraction of CB increased. Consequently, less matrix material was available for load bearing during the compression test. Similar deterioration in compressive strength was reported for Mg-based foams [29,38,39] due to an increase in porosity.

Comparing the two groups of samples in this work, the HS-samples from *Group 1* presented a better combination of compressive strength and energy absorption characteristics. Typically, the samples tested in this study exhibited an onset of plateau stress at about 10% strain. The relationship between the peak compressive strength and density of the syntactic foams in this study and some previous studies [18,19,40], is plotted in Fig. 5. The values of the peak strength were extracted from the compressive stress-strain curves for some studies that did not directly provide such data. One of the advantages of hybridising cell structure is that it can be used to tailor the properties of a foam towards specialised applications. For instance, with proper design calculations, a density less than that of water can be achieved. Such foams are potential materials for buoyancy applications.

Other than the reports in Refs. [18, 19, 40] on Al- and Zn-alloy syntactic foams and the current study, a density of 0.97 g/cm^3 was previously reported for an Mg alloy AZ91D/SiC syntactic foam fabricated via

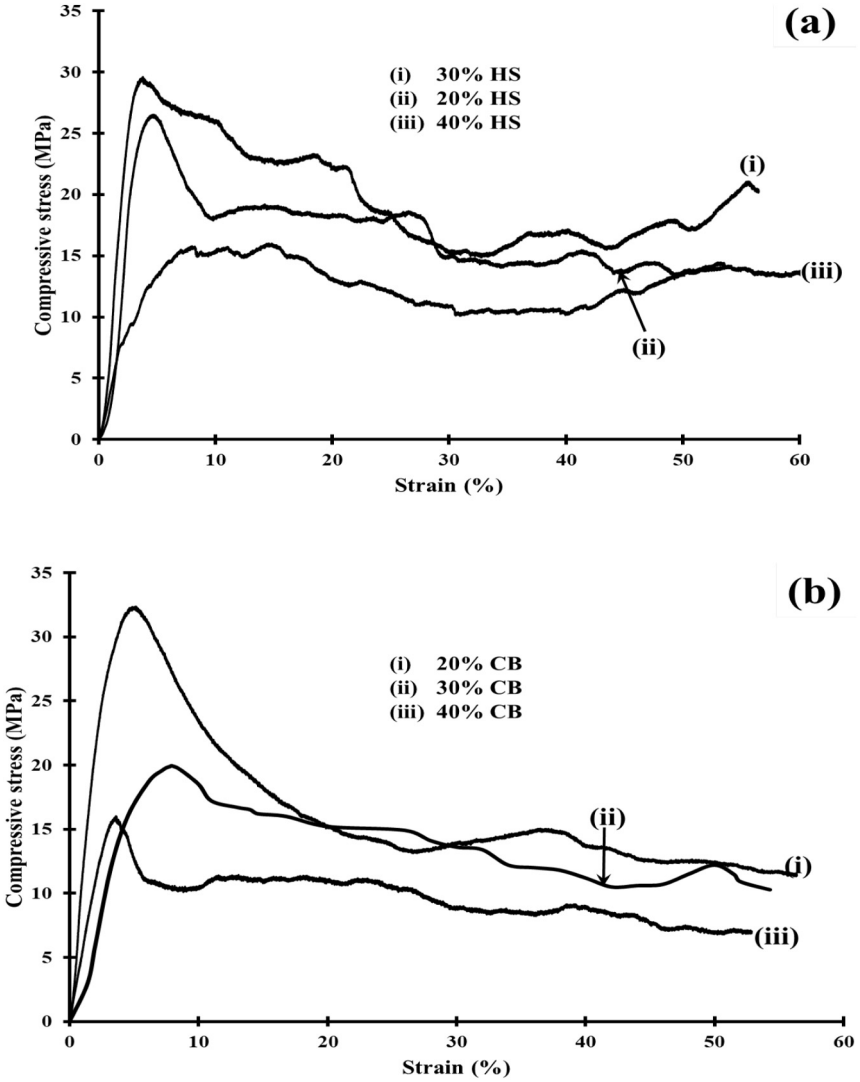

Fig. 4. Representative stress-strain graphs of composite foam with various (a) volume fraction of hollow spheres (HS) and (b) volume fraction of carbamide (CB).

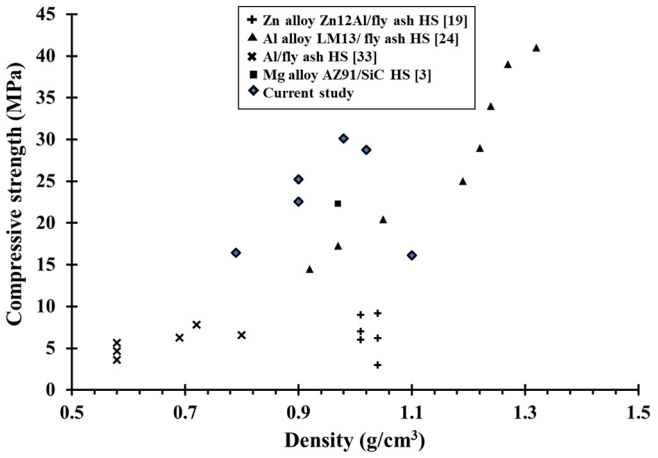

Fig. 5. Comparison of peak compressive strengths between different hybrid syntactic foams.

the pressure infiltrated method [1]. From Fig. 5, the compressive strength increased with an increase in density. It is noted that AZ61 hybrid syntactic foam was less dense than a similar Mg alloy AZ91D/SiC syntactic foam [1]. Within the same density range, the peak compressive strengths measured in the current study were at least similar, and in most cases, higher than those of Zn [18], AZ91D [1], and Al [19,40] syntactic foams. The improved strength realized in this present work can be attributed to the processing technique utilised in this study. The rapid sintering characteristic of MW can minimise the formation of brittle interfacial products between the matrix and fly ash particles, which are detrimental to the strength of the samples. This is difficult to achieve using the melt processing that is characterised by prolong contact time between molten Al and fly ash particles. This invariably encourages undesired reactions that form brittle interfacial products. The hybrid syntactic foams in Ref. [40], with densities lower than 0.80 g/cm^3, had considerably lower compressive strengths, below 10 MPa. The Mg alloy hybrid syntactic foams reported in our study shows the potential to reduce structural weight by replacing Al- and Zn-based foams. This current investigation is therefore the first systematic study on exploiting the potentials of PM and MW sintering techniques for developing low density Mg-based syntactic foams.

3.4. Results of buoyancy and contact angle tests

The syntactic foam sample with 40% CB (density = 0.79 g/cm^3) from *Group 2* showed remarkable floatability (see Video 1) due to its hybrid pore structure and low density. Unlike some earlier reports on floatable metallic foams [24,41] and metallic microboats [20,26], no surface treatments were required to induce superhydrophobicity in this study. The result of the static water contact angle (CA) measurement is shown in Fig. 6.

The polished surface of a sintered AZ61 sample, in Fig. 6(a), was relatively flat and smooth and showed no prominent hierarchical or rough features that are characteristic of chemically-induced superhydrophobic surfaces [25,42]. The CA of the surface was evaluated as 45 ± 2° (Fig. 7b), an indication that it was hydrophilic. This result is in consonance with the 44.50° reported for the CA of the surface of an AZ31 magnesium alloy [42]. Despite this hydrophilic characteristic, the sample in the present study was still able to float on water due to its low-density hybrid cell structure.

3.5. Potential applications as a microboat and chemical release agent

3.5.1. Marangoni-induced propulsion of microboat

The shape and dimensions of a microboat (0.15 g) machined from the floatable sample are shown in Fig. 7.

The circular slot at the back of the microboat housed a tiny polymeric foam (3.80 mg), which served as a reservoir for the ethanol propellant. When the microboat, loaded with its propellant, was placed in the water tank, a spontaneous locomotion was observed, as shown in Video 2. The mechanism of propulsion could be ascribed to the Marangoni effect [21,22], arising from the difference in the surface tension of water between the fore and aft of the microboat. When ethanol diffused into water at the aft of the microboat, the surface tension of water was lowered compared to its value at the fore of the microboat. Consequently, a surface tension gradient was generated and caused the microboat to move forward towards the region of a higher surface tension. A similar mechanism was reported for an aerogel membrane [21] and a PDMS microboat [22].

3.5.2. Chemical release agent: estimation of the volumetric flow rate of ethanol propellant

Bulk delivery is one of the principal ways by which drugs are delivered in drug delivery systems [43]. Some previous studies have reported a drug delivery system based on Mg foams [44]. Drugs are loaded into the foam, while its morphology and pore volume fraction control the release rate. In the previous section, it has been shown that the hybrid syntactic foam synthesised in this study can be autonomously propelled by ethanol. Similarly, controlled release of drugs may be achieved when ethanol is replaced with the desired drug. This concept is demonstrated in this study by using ethanol dyed with a blue ink and its gradual release is studied.

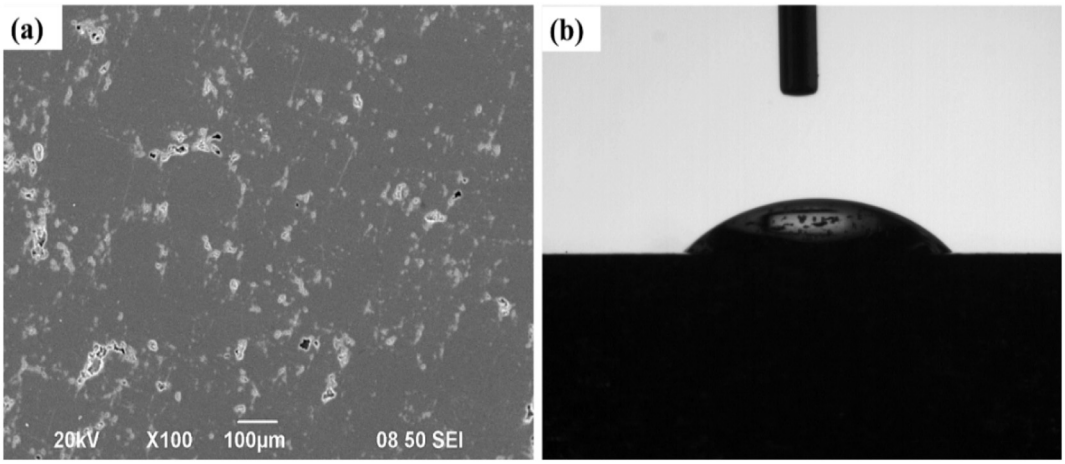

Fig. 6. (a) SEM image of the surface of sintered and polished bulk AZ61 magnesium alloy (b) Image of the static water contact angle on the polished surface of (a).

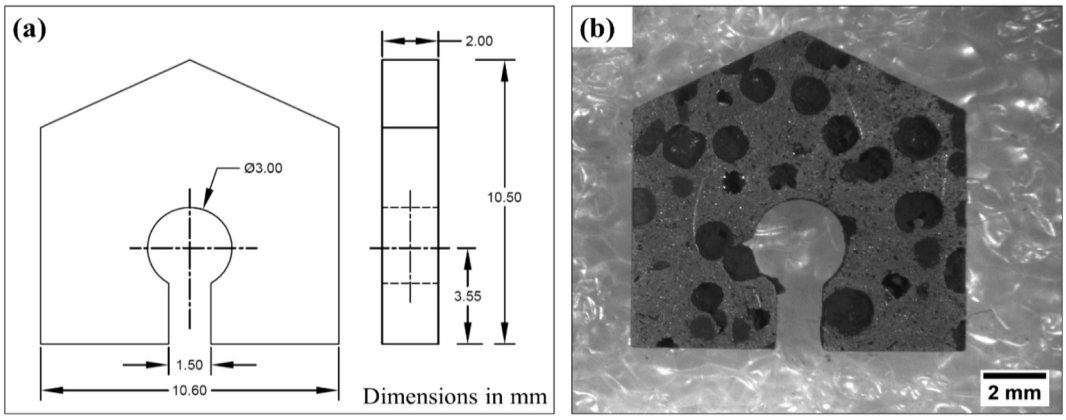

Fig. 7. (a) CAD drawing of the microboat showing its dimensions in mm (b) An optical image of a microboat machined from the AZ61 hybrid foam sample.

Fig. 8 shows the image sequence of the displacement of the outer edge of 80% v/v dyed ethanol. Between Fig. 8(a) and (b), the edge (black arrow in Fig. 8) was displaced by 8.52 mm in 0.12 s, which corresponded to a velocity of 71 mm/s. Subsequent calculations showed that the velocity decreased to ~20, 19, 18 and 17 mm/s in Fig. 8(c), (d), (e), and (f), respectively. This showed the velocity of the displaced ethanol decreased as its distance from the origin (i.e. the slot at the back of the microboat) increased. These results agreed with the results of ethanol spreading experiments earlier described by some authors [45]. Moreover, this experiment also indicates the potential application of the syntactic foam as a chemical release agent.

A summary of the maximum velocity (v_{max}) against ethanol concentration (c) is plotted in Fig. 9. From the plot, v_{max} increased with increasing concentration of ethanol. The highest v_{max} was about 114 mm/s at 100% v/v ethanol, whereas the lowest v_{max} was approximately 82 mm/s at a concentration of 80% v/v. An expression relating c to v_{max}, can be extracted from the plot as:

$$v_{max} = 21\ exp0.017c \tag{7}$$

A simple model was proposed to estimate the volumetric flow rate, Q of ethanol as it exits the aft of the microboat. Taking A to be the area of the slot (3 mm^2) from which ethanol diffused into water, the volumetric flow rate can be expressed as:

$$Q = v_{max}A \tag{8}$$

Therefore, the values of Q for 100, 90, and 80% v/v ethanol were 349, 294, and 248 mm^3/s. These results indicated that the estimated flow rate decreased with decreasing concentration of ethanol.

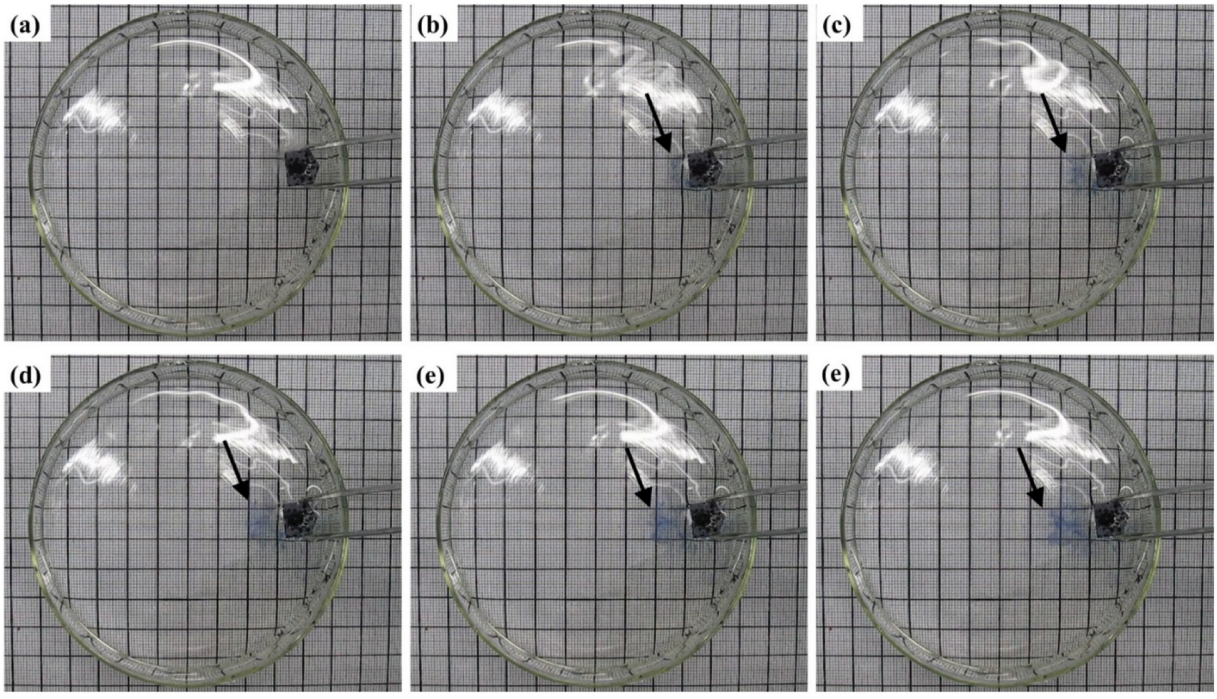

Fig. 8. Image sequence of the displacement of the leading edge of 80% v/v ethanol (dyed with a blue ink) away from the microboat. The displacement of the leading edge (indicated by the black) starts in (a) and ends in (f). The time between each image is 0.12 s. Each grid is a square of 10 × 10 mm^2.

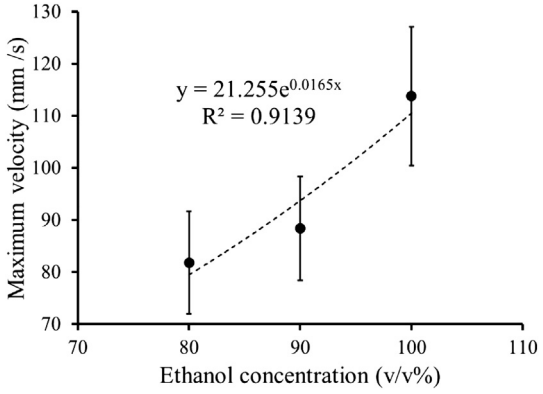

Fig. 9. Plot of maximum flow velocity (v_{max}) against ethanol concentration (c).

4. Conclusions

Powder metallurgy and rapid microwave sintering techniques were successfully applied to hybridize the cell structure of magnesium alloy AZ61 syntactic foams. Hybrid closed- and open-cells were realized from leached carbamide granules and fly ash hollow microspheres, respectively. This cell hybridisation technique was utilised to reduce density and realize adequate strength in the syntactic foams. Accordingly, floatable foams with a density of about 0.79 g/cm^3 and compressive strength of 16 MPa were synthesised without recourse to any surface modification or chemically-induced superhydrophobicity. The processing techniques mitigated damage to the fly ash hollow particles as confirmed by the microstructural examinations. Microwave sintering was rapidly completed within 20 min, thus interfacial reactions were suppressed, and significant energy and time savings were realized. Surface wetting test indicated that the surface of the foam was hydrophilic, thus supporting the experimental results that buoyancy was achieved due to the hybrid cell structure and low density of the syntactic foam sample. Furthermore, potential applications of the floatable syntactic foam sample as a microboat and chemical release agent were demonstrated, using ethanol as a propellant. A simple model was also proposed to estimate the volumetric flow rate of the propellant. The results from this study demonstrated a new technique for designing floatable metallic structures without the need for chemical and/or surface modifications, thus extending the group of "floatable" materials to metals and their application fields.

Supplementary data to this article can be found online at https://doi.org/10.1016/j.matdes.2018.10.004.

CRediT authorship contribution statement

Akeem Damilola Akinwekomi: Designed and conducted the experiments, Collected the data and analysed the results. **Ling Chen:** Designed and conducted the experiments, Collected the data and analysed the results. **Chak-Yin Tang:** Generated the idea, Analysed the data and prepared the manuscript. **Gary Chi-Pong:** Prepared the manuscript and the revision. **Wing-Cheung Law:** Prepared the manuscript and the revision. **Xu-Sheng Yang:** Prepared the manuscript and the revision. **Mohd Hamdi:** Prepared the manuscript and the revision.

Acknowledgment

This work was fully supported by the Hong Kong PhD Fellowship Scheme (Project Code 1-904Z).

References

[1] H. Anantharaman, V.C. Shunmugasamy, O.M. Strbik, N. Gupta, K. Cho, Dynamic properties of silicon carbide hollow particle filled magnesium alloy (AZ91D) matrix syntactic foams, Int. J. Impact Eng. 82 (2015) 14–24.
[2] Q.B. Nguyen, M.L. Sharon Nai, A.S. Nguyen, S. Seetharaman, E.W. Wai Leong, M. Gupta, Synthesis and properties of light weight magnesium–cenosphere composite, Mater. Sci. Technol. 32 (2016) 923–929.
[3] N.N. Lu, X.J. Wang, L.L. Meng, C. Ding, W.Q. Liu, H.L. Shi, X.S. Hu, K. Wu, Electromagnetic interference shielding effectiveness of magnesium alloy-fly ash composites, J. Alloys Compd. 650 (2015) 871–877.
[4] Q. Li, G. Jiang, J. Dong, J. Hou, G. He, Damping behavior and energy absorption capability of porous magnesium, J. Alloys Compd. 680 (2016) 522–530.
[5] B.P. Neville, A. Rabiei, Composite metal foams processed through powder metallurgy, Mater. Des. 29 (2008) 388–396.
[6] C.A. Vogiatzis, S.M. Skolianos, On the sintering mechanisms and microstructure of aluminium–ceramic cenospheres syntactic foams produced by powder metallurgy route, Compos. A: Appl. Sci. Manuf. 82 (2016) 8–19.
[7] S. Sankaranarayanan, Q.B. Nguyen, R. Shabadi, A.H. Almajid, M. Gupta, Powder metallurgy hollow fly ash cenospheres' particles reinforced magnesium composites, Powder Metall. 59 (2016) 188–196.
[8] X. Xia, J. Feng, J. Ding, K. Song, X. Chen, W. Zhao, B. Liao, B. Hur, Fabrication and characterization of closed-cell magnesium-based composite foams, Mater. Des. 74 (2015) 36–43.
[9] L.C. Zou, Q. Zhang, B.J. Pang, G.H. Wu, L.T. Jiang, H. Su, Dynamic compressive behavior of aluminum matrix syntactic foam and its multilayer structure, Mater. Des. 45 (2013) 555–560.
[10] C.A. Vogiatzis, A. Tsouknidas, D.T. Kountouras, S. Skolianos, Aluminum-ceramic cenospheres syntactic foams produced by powder metallurgy route, Mater. Des. 85 (2015) 444–454.
[11] Z. Huang, S. Yu, Microstructure characterization on the formation of in situ Mg_2Si and MgO reinforcements in AZ91D/Flyash composites, J. Alloys Compd. 509 (2011) 311–315.
[12] D.B. Newsome, B.F. Schultz, J.B. Ferguson, P.K. Rohatgi, Synthesis and quasi-static compressive properties of Mg-AZ91D-Al_2O_3 syntactic foams, Arch. Math. 8 (2015) 6085–6095.
[13] J. Čapek, D. Vojtěch, Properties of porous magnesium prepared by powder metallurgy, Mater. Sci. Eng. C 33 (2013) 564–569.
[14] D.P. Mondal, J. Datta Majumder, N. Jha, A. Badkul, S. Das, A. Patel, G. Gupta, Titanium-cenosphere syntactic foam made through powder metallurgy route, Mater. Des. 34 (2012) 82–89.
[15] A.D. Akinwekomi, W.-C. Law, C.-Y. Tang, L. Chen, C.-P. Tsui, Rapid microwave sintering of carbon nanotube-filled AZ61 magnesium alloy composites, Compos. Part B Eng. 93 (2016) 302–309.
[16] A.D. Akinwekomi, W.-C. Law, M.-T. Choy, L. Chen, C.-Y. Tang, G.C.-P. Tsui, X.-S. Yang, Processing and characterisation of carbon nanotube-reinforced magnesium alloy composite foams by rapid microwave sintering, Mater. Sci. Eng. A 726 (2018) 82–92.
[17] Y. Wan, T. Cui, W. Li, C. Li, J. Xiao, Y. Zhu, D. Ji, G. Xiong, H. Luo, Mechanical and biological properties of bioglass/magnesium composites prepared via microwave sintering route, Mater. Des. 99 (2016) 521–527.
[18] A. Daoud, Effect of strain rate on compressive properties of novel Zn12Al based composite foams containing hybrid pores, Mater. Sci. Eng. A 525 (2009) 7–17.
[19] D.P. Mondal, N. Jha, B. Gull, S. Das, A. Badkul, Microarchitecture and compressive deformation behaviour of Al-alloy (LM13)-cenosphere hybrid Al-foam prepared using $CaCO_3$ as foaming agent, Mater. Sci. Eng. A 560 (2013) 601–610.
[20] M. Xiao, X. Guo, M. Cheng, G. Ju, Y. Zhang, F. Shi, pH-responsive on-off motion of a superhydrophobic boat: towards the design of a minirobot, Small 10 (2014) 859–865.
[21] H. Jin, A. Marmur, O. Ikkala, R.H.A. Ras, Vapour-driven Marangoni propulsion: continuous, prolonged and tunable motion, Chem. Sci. 3 (2012) 2526.
[22] C. Luo, H. Li, L. Qiao, X. Liu, Development of surface tension-driven microboats and microflotillas, Microsyst. Technol. 18 (2012) 1525–1541.
[23] L. Qiao, D. Xiao, F.K. Lu, C. Luo, Control of the radial motion of a self-propelled microboat through a side rudder, Sensors Actuators A Phys. 188 (2012) 359–366.
[24] K. Ji, J. Liu, J. Zhang, J. Chen, Z. Dai, Super-floatable multidimensional porous metal foam integrated with a bionic superhydrophobic surface, J. Mater. Chem. A 2 (2014) 16589–16593.
[25] X. Zhang, J. Zhao, Q. Zhu, N. Chen, M. Zhang, Q. Pan, Bioinspired aquatic microrobot capable of walking on water surface like a water strider, ACS Appl. Mater. Interfaces 3 (2011) 2630–2636.
[26] A. Musin, R. Grynyov, M. Frenkel, E. Bormashenko, Self-propulsion of a metallic superoleophobic micro-boat, J. Colloid Interface Sci. 479 (2016) 182–188.
[27] N. Murayama, H. Yamamoto, J. Shibata, Mechanism of zeolite synthesis from coal fly ash by alkali hydrothermal reaction, Int. J. Miner. Process. 64 (2002) 1–17.
[28] E. Meijering, O. Dzyubachyk, I. Smal, Methods for cell and particle tracking, in: P.M. Conn (Ed.), Methods Enzymol, Elsevier 2012, pp. 183–200.
[29] Y. Bi, Y. Zheng, Y. Li, Microstructure and mechanical properties of sintered porous magnesium using polymethyl methacrylate as the space holder, Mater. Lett. 161 (2015) 583–586.
[30] D.J. Lloyd, Particle reinforced aluminium and magnesium matrix composites, Int. Mater. Rev. 39 (1994) 1–23.
[31] F. Moll, K.U. Kainer, Particle-reinforced magnesium alloys, in: K.U. Kainer (Ed.), Magnes. Alloy. Technol, Wiley-VCH Verlag GmbH & Co. KGaA, Weinheim, Germany, 2003.
[32] Y.P. Hung, J.C. Huang, K.J. Wu, C.Y.A. Tsao, Strengthening and toughness of AZ61 Mg with nano SiO_2 particles, Mater. Trans. 47 (2006) 1985–1993.
[33] X. Wang, Z. Li, Y. Huang, K. Wang, X. Wang, F. Han, Processing of magnesium foams by weakly corrosive and highly flexible space holder materials, Mater. Des. 64 (2014) 324–329.
[34] H. Zhuang, Y. Han, A. Feng, Preparation, mechanical properties and in vitro biodegradation of porous magnesium scaffolds, Mater. Sci. Eng. C 28 (2008) 1462–1466.

[35] A. Daoud, M. Abouelkhair, M. Abdelaziz, P. Rohatgi, Fabrication, microstructure and compressive behavior of ZC63 Mg–microballoon foam composites, Compos. Sci. Technol. 67 (2007) 1842–1853.
[36] M.N. Rahaman, Ceramic Processing, CRC/Taylor & Francis, 2007.
[37] L. Lu, M.O. Lai, M.L. Hoe, Formation of nanocrystalline Mg_2Si and Mg_2Si dispersion strengthened Mg-Al alloy by mechanical alloying, Nanostruct. Mater. 10 (1998) 551–563.
[38] C.E. Wen, Y. Yamada, K. Shimojima, Y. Chino, H. Hosokawa, M. Mabuchi, Compressibility of porous magnesium foam: dependency on porosity and pore size, Mater. Lett. 58 (2004) 357–360.
[39] H. Cay, H. Xu, Q. Li, Mechanical behavior of porous magnesium/alumina composites with high strength and low density, Mater. Sci. Eng. A 574 (2013) 137–142.
[40] X. Xia, X. Chen, Z. Zhang, X. Chen, W. Zhao, B. Liao, B. Hur, Compressive properties of closed-cell aluminum foams with different contents of ceramic microspheres, Mater. Des. 56 (2014) 353–358.
[41] X. Jin, B. Shi, L. Zheng, X. Pei, X. Zhang, Z. Sun, Y. Du, J.H. Kim, X. Wang, S. Dou, K. Liu, L. Jiang, Bio-inspired multifunctional metallic foams through the fusion of different biological solutions, Adv. Funct. Mater. 24 (2014) 2721–2726.
[42] T. Zheng, Y. Hu, Y. Zhang, F. Pan, Formation of a hydrophobic and corrosion resistant coating on magnesium alloy via a one-step hydrothermal method, J. Colloid Interface Sci. 505 (2017) 87–95.
[43] J.A. Lyndon, B.J. Boyd, N. Birbilis, Metallic implant drug/device combinations for controlled drug release in orthopaedic applications, J. Control. Release 179 (2014) 63–75.
[44] E. Aghion, T. Yered, Y. Perez, Y. Gueta, The prospects of carrying and releasing drugs via biodegradable magnesium foam, Adv. Eng. Mater. 12 (2010) B374–B379.
[45] D.G. Suciu, O. Smigelschi, E. Ruckenstein, The spreading of liquids on liquids, J. Colloid Interface Sci. 33 (1970) 520–528.